Establishing a Statistical Link Between Network Oscillations and Neural Synchrony

Pengcheng Zhou*
Center for the Neural Basis of Cognition
Machine Learning Department
Carnegie Mellon University,
Pittsburgh, PA, 15213, USA

Abstract

Background: Pairs of active neurons frequently fire action potentials or "spikes" nearly synchronously (i.e., within 5 ms of each other). This spike synchrony may occur by chance, based solely on the neurons' fluctuating firing patterns, or it may occur too frequently to be explicable by chance alone. When spike synchrony above chance levels is present, it may subserve computation for a specific cognitive process, or it could be an irrelevant byproduct of such computation. However, we still lack knowledge of how this synchrony is generated.
Aim: Network-wide oscillations are an important possible source of spike synchrony, and may be an essential mechanism of network information flow. In the neuroscience community, there is a hypothesis suggesting that neurons communicate through coherent oscillations, which can be recorded in local field potential. In this work, we aim to develop a statistical framework to test this hypothesis.
Data: We used ground truth knowledge of simulated data to test the proposed method, and we also illustrated the application of this method using two experimentally recorded datasets: *in vitro* recordings of rat hippocampal CA1 pyramidal cells, and *in vivo* recordings of neocortical V4 neurons from a behaving monkey. For each dataset, we have spike trains and oscillatory signals of two neurons over multiple trials.
Methods: A point process regression framework, implemented via generalized linear models (GLMs), has been previously developed for this purpose. In this framework, the observed number of synchronous spikes is compared to the number predicted by chance under varying assumptions about the factors that affect each of the individual neurons' firing-rate functions. To establish the statistical link between spike synchrony and network-wide oscillations, we integrated oscillatory field potentials into our point process regression framework. We then used this new framework to demonstrate the statistical relationship between oscillatory field potentials and spike synchrony.
Results: (1) Our new point process regression model can perfectly recover the the phase relationships between oscillatory field potentials and firing rates; (2) In both simulated and experimental data, our proposed framework can successfully identify the contribution of oscillations to spike synchrony.
Conclusions: In this article, we provide a method for establishing the statistical association between spike synchrony and an oscillatory local field potential. We demonstrate the value of this technique by numerical simulation together with application to both *in vitro* and *in vivo* neural recordings. It could be a powerful tool for testing one specific scientific hypothesis in neuroscience research.

*in collaboration with Shawn D. Burton, Adam C. Snyder, Matthew A. Smith, Nathaniel N. Urban, and Robert E. Kass

1 Introduction

A leading theory of current neuroscience is that synchronous firing of neurons driven by network-wide oscillations may encode and transmit information within and across brain regions [Brette, 2012,Colgin et al., 2009, Engel et al., 2001, Fries, 2005, Geman, 2006, Niebur et al., 2002, Salinas and Sejnowski, 2001, Sejnowski and Paulsen, 2006, Tiesinga et al., 2008]. Supporting this theory, a number of studies have suggested that synchronous firing of action potentials or "spikes" may indeed occur in conjunction with oscillations in local field potentials (LFP) [Denker et al., 2011, Friedrich et al., 2004, Gregoriou et al., 2009, Mizuseki and Buzsaki, 2014, Robbe et al., 2006]. However, a missing link in this theory has been the ability to dissociate enhanced spike synchrony due to network-wide oscillations from enhanced spike synchrony that may be due to other measured or unmeasured sources. Recently, we developed a statistical framework in which the association between spike synchrony and measured covariates may be assessed [Kass et al., 2011,Kelly and Kass, 2012]. Here we show how this approach may be applied to describe the relationship between spike synchrony and oscillatory activity.

2 Problem description

The aim of this project is to design a statistical framework connecting network oscillations and neural synchrony. Given the spike trains corresponding to a pair of neurons and local, but wider-scale, oscillatory signals, the proposed the proposed method is determines to tell us whether the pairwise spike synchrony is modulated by the network-wide oscillation. In addressing this problem, we need a quantitative model of how an oscillating signal may modulate a single neuron's firing rate.

3 Background

This work attempts to solve a specific biological question currently of interest to the neuroscience community. We will first define a few terms, which will be necessary background for the remainder of the paper.
Action potential: An action potential is a short-lasting event in which the electrical potential of a neuron rapidly rises and falls (over a duration of roughly one millisecond), and follow a very stereotyped trajectory specific to the individual cell. It is also called a 'spike' due to the sharp form of the membrane potential's trace. A sequence of spikes is called a spike train, which can be conceptualized as a series of discrete events (0 or 1) within continuous time. A spike train can therefore be modeled naturally as a point process.
Local Fields Potentials (LFP): LFP is an electrophysiological signal measuring an electrical current flowing across a small volume of neural tissue, thought to be generated by multiple spiking neurons diffusing ions in the process of their communication. We can observe oscillations in LFPs and these oscillations represent population activity within a network. Local field potentials can be recorded simultaneously with spike trains using extracellular recording.
Phase modulation: Many researchers have reported that firing rate is modulated by the phase of specific network-wide oscillations in different brain areas, such as monkey V1 [Jia et al., 2013], rat hippocampus [Sirota et al., 2008], and rat prefrontal cortex [Siapas et al., 2005]. These studies used spike phase histograms to show this phase modulation. The significance of phase locking can be evaluated using Rayleigh's Z statistic [Siapas et al., 2005].
Spike synchrony: spike synchrony will be defined as instances where neurons fire within the same small temporal bin ($\sim$ 5 ms). This could happen randomly, but it could also reflect coordinated neuronal activity on a fine time scale.

Our lab has developed a statistical framework to assess the association between spike synchrony and a measured covariate [Kass et al., 2011, Kelly and Kass, 2012]. My work is based on this framework and focuses specifically on the network-wide oscillation extracted from the measured LFP. Using point process regression models, which take the form of generalized linear models (GLMs), our statistical framework compares the observed number of synchronous spikes within a small time window (here, 5 ms) to the number predicted by chance, under varying assumptions about the factors that affect the firing of each individual neuron [Kass et al., 2011, Kelly and Kass, 2012]. The number of synchronous spikes predicted "by chance" refers here to the number predicted under conditional

independence after conditioning on the various measured factors that have been hypothesized to affect individual-neuron spiking. For example, two neurons with fluctuating stimulus-driven firing rates will produce some number of synchronous spikes even if they are acting independently. The point process regression method fits fluctuating firing rate functions for each neuron separately, then predicts the number of synchronous spikes under conditional independence (i.e., after conditioning on these fluctuating firing rates), and compares the prediction to the observed number of synchronous spikes. By this method, a single factor may be either included or excluded from the regression model in order to quantify that factor's ability to explain the observed spike synchrony.

4 Approach

In this article, we consider the contribution of network-wide oscillations by comparing observed and predicted spike synchrony after conditioning on the phase of an LFP representing a network-wide oscillation. Thus, we predict spike synchrony with and without inclusion of LFP phase as an explanatory variable for each neuron separately. To demonstrate that increased spike synchrony is associated with a network-wide oscillation, we would begin by establishing that, without considering LFP phase, the observed number of synchronous spikes is greater than the predicted number by a statistically significant magnitude, after conditioning on both stimulus-driven firing rates and recent post-spike history effects. This would indicate a failure of the phase-free model to accurately account for spike synchrony. We would then include the LFP phase in the model, and if it succeeded in predicting spike synchrony, then we would conclude that LFP phase can explain the remaining spike synchrony. Furthermore, we could estimate the proportion of excess synchronous spikes accounted for by the LFP phase. The same procedure could be used, instead to demonstrate the role of network-wide oscillations in suppressing spike synchrony.

In order to carry out this general procedure, we first need to model an individual neuron's spiking probability in terms of LFP phase. We follow [Lepage et al., 2013], which recently described and assessed point process regression models that include a sinusoidal phase term. We enhance their approach by weakening the sinusoidal assumption, allowing the phase relationship to be nonparametric as in [Kaufman et al., 2005]. Using this point process regression model, we are then able to quantify the dependence of synchronous spiking on an oscillatory modulation. We illustrate the method using simulated neurons, *in vitro* recordings of hippocampal CA1 pyramidal cells, and *in vivo* recordings of neocortical V4 neurons from a behaving monkey.

5 Materials and Methods

5.1 Point-Process Framework

In a continuous time interval $(0, T]$, a neuron can fire a spike at any discrete time point u_i. A series of spikes $\{u_i\}$ for $1 \leq i \leq N$ forms the spike train, where $0 \leq u_1 < \cdots < u_N \leq T$. We take the spike train to be a point process, which is characterized by its conditional intensity function

$$\lambda(t|H_t, X_t) = \lim_{\Delta \to 0} \frac{P\left[N(t+\Delta) - N(t) = 1 | H_t, X_t\right]}{\Delta} \tag{1}$$

where $N(t)$ is the total number of spikes prior to time t, H_t is neuron's own spiking history prior to time t, and X_t includes all other relevant covariates. When Δ is small, $\lambda(t|H_t, X_t) \cdot \Delta$ approximates to the firing probability in the time interval $(t, t+\Delta)$. To determine how different factors contribute to firing rate we write $\lambda(t|H_t, X_t)$ as a function of (H_t, X_t)

$$\lambda(t|H_t, X_t) = f(H_t, X_t). \tag{2}$$

We can include different factors into this model and study their effects. Usually the stimulus $S(t)$ is included when neurons show selectivity to stimuli. In this work, because we are interested in phase modulation by an oscillatory signal, the phase of the specific oscillation $\Phi(t)$ is also included.

5.2 Generalized Linear Model

To take advantage of the generalized linear model (GLM) framework we divide T into K equally spaced bins, thus taking the bin width to be $\Delta = T/K$. Δ is small enough that no more than one

spike event in each bin, e.g. $\Delta = 1$ ms. Therefore the probability of observing one spike in kth bin is

$$p_k = \lambda(t_k|H_{t_k}, X_{t_k}) \cdot \Delta, \qquad k = 1, 2, \cdots, K \tag{3}$$

Using the vector $Y \subset \mathbb{R}^{K\times 1}$ to represent the spike train $\{u_i\}$, y_k is the number of spikes in kth bin. Since we choose small bin width Δ, y_k is not bigger than 1, i.e. $y_k \in \{0, 1\}$ and, from the Poisson approximation to the binomial for small p we take the probability of observing y_k given H_{t_k} and X_{t_k} to be

$$p(y_k|H_{t_k}, X_{t_k}) = \frac{p_k^{y_k}}{y_k!} e^{-p_k} \tag{4}$$

where $t_k = k\Delta$. The loglikelihood function is

$$L = \sum_{k=1}^{K} [y_k \cdot \log(p_k) - p_k] = \sum_{k=1}^{K} [y_k \cdot \log(\lambda(t_k|H_{t_k}, X_{t_k})\Delta) - \lambda(t_k|H_{t_k}, X_{t_k})\Delta] \tag{5}$$

and this is maximized to determine the MLE fit.

We assume that $\log[\lambda(t|H_t, X_t)]$ can be written as a sum of specific functions of each covariate. Here we are studying three factors, stimulus, recent post-spike auto-history, and oscillatory phase, and we write

$$\log[\lambda(t|H_t, X_t)] = f_1(\text{stimulus}) + f_2(\text{auto-history}) + f_3(\text{oscillation}) \tag{6}$$

$$= f_1(S_t) + f_2(H_t) + f_3(\Phi_t). \tag{7}$$

Here, $S(t)$ is a possibly time-varying stimulus and $f_1(\text{stimulus})$ determines the trial-independent time-varying firing rate, i.e., the effect that is usually associated with the peri-stimulus time histogram (the PSTH), which may be estimated due to the repeated trial structure of the experiment. The recent post-spike auto-history effect is assumed here to be dominated by effects subsequent to the most recent spike t^* prior to time t, as in [Kass and Ventura, 2001], so we assume $f_2(\text{auto-history})$ has the form $f_2(t - t^*)$. The oscillatory term $f_3(\text{oscillation})$ is defined as $f_3(\Phi_t)$, where Φ_t is the phase of specific oscillation. In summary, our spike train model has the form

$$\log(\lambda(t|H_t, X_t)) = f_1(t) + f_2(t - t^*) + f_3(\Phi_t) \tag{8}$$

$$= \log\lambda_1(t) + \log\lambda_2(t - t^*) + \log\lambda_3(\Phi_t) \tag{9}$$

and we will assume $f_1(\cdot)$, $f_2(\cdot)$ and $f_3(\cdot)$ are smooth functions.

The model in Equation (9) is a "full" model including stimulus, auto-history, and an oscillatory factor. Importantly, we can remove selected factors from the full model (e.g., the LFP phase modulation) and still fit the spike trains using the same procedure. Indeed, in the following results, we also fit a simplified model lacking the oscillatory factor,

$$\log\lambda(t|H_t, X_t) = \log\lambda_1(t) + \log\lambda_2(t - t^*). \tag{10}$$

5.3 Spike Synchronization

For a pair of neurons labeled 1 and 2, we fit conditional firing rate for each of them to get $\hat{\lambda}_1(t|H_t, X_t)$ and $\hat{\lambda}_2(t|H_t, X_t)$. Then we can predict the number of synchronized spikes given temporal bins with $\Delta = 5$ ms, as in [Kass et al., 2011], using

$$N_{pred} = \int \hat{\lambda}_1(t|H_t, X_t) \cdot \hat{\lambda}_2(t|H_t, X_t)dt. \tag{11}$$

Given spike trains from these two neurons, we can also get the observed number of synchronized spikes N_{obs} by counting. If a pair of spikes from two neurons has an time interval less than 5 ms, then this pair is counted as a synchronized spike. Synchrony is measured by taking the ratio of these two numbers $\hat{\zeta}$ or $\log\hat{\zeta}$

$$\hat{\zeta} = \frac{N_{obs}}{N_{pred}}. \tag{12}$$

When two neurons are conditional independent, equation (11) can make relative good predictions and $\hat{\zeta} \approx 1$ (or $\log\hat{\zeta} \approx 0$). We can use parametric bootstrap to test the null hypothesis $H_0 : \log\zeta = 0$ and check the conditional independence between two neurons.

5.4 Acute slice electrophysiology

Experiments were completed in compliance with the guidelines established by the Institutional Animal Care and Use Committee of Carnegie Mellon University. Whole-cell patch clamp recordings of hippocampal CA1 pyramidal cells were performed similar to previously described methods [Burton and Urban, 2014]. Briefly, a postnatal day 16 Thy1-YFP-G mouse [Feng et al., 2000] was anesthetized with isoflurane and decapitated into ice-cold oxygenated dissection solution containing (in mM): 125 NaCl, 25 glucose, 2.5 KCl, 25 $NaHCO_3$, 1.25 NaH_2PO_4, 3 $MgCl_2$ and 1 $CaCl_2$. Brains were rapidly isolated and sagittal slices (310 μm thick) containing the hippocampus were cut using a vibratome (5000 mz-2; Campden, Lafayette, IN, USA). Slices recovered for $\sim$ 30 min in $\sim$ 37C oxygenated Ringer solution that was identical to the dissection solution except for lower Mg^{2+} concentrations (1 mM $MgCl_2$) and higher Ca^{2+} concentrations (2 mM $CaCl_2$). Slices were then stored in room temperature oxygenated Ringer solution until recording. During recording, slices were continuously superfused with warmed oxygenated Ringer's solution (temperature measured in bath: 32ºC). CA1 pyramidal cells were identified by morphology and laminar position using infrared differential interference contrast microscopy. Whole-cell recordings were made using electrodes (final electrode resistance: $5 - 7$ MΩ) filled with (in mM): 120 potassium gluconate, 2 KCl, 10 Hepes, 10 sodium phosphocreatine, 4 Mg-ATP, 0.3 Na_3GTP, 0.2 EGTA, 0.25 Alexa Fluor 594 (Life Technologies, Carlsbad, CA, USA) and 0.2% Neurobiotin (Vector Labs, Burlingame, CA, USA). The liquid junction potential was $12 - 14$ mV and was not corrected for. Pipette capacitance was carefully neutralized and series resistance was compensated using the MultiClamp Bridge Balance operation. Data were low-pass filtered at 4 kHz and digitized at 10 kHz using a MultiClamp 700A amplifier (Molecular Devices, Sunnyvale, CA, USA) and an ITC-18 acquisition board (Instrutech, Mineola, NY, USA) controlled by custom software written in Igor Pro (WaveMetrics, Lake Oswego, OR, USA). Cell morphology was reconstructed under a 100X oil-immersion objective and analyzed with Neurolucida (MicroBrightField, Inc., Williston, VT, USA).

5.5 V4 neurons

Experimental procedures were approved by the Institutional Animal Care and Use Committee of the University of Pittsburgh. A separate analysis of these data has been previously reported ([Snyder et al., 2015, Snyder and Smith, 2015]).

Subjects: We implanted one, 100-electrode "Utah" array (Blackrock Microsystems) in right V4 in one adult male rhesus macaque (*Macaca mulatta*). The basic surgical procedures have been described previously [Smith and Sommer, 2013], and were conducted in aseptic conditions under isoflurane anesthesia. In addition to the microelectrode arrays, the animal was implanted with a titanium head post to immobilize the head during experiments. We recorded neurons with receptive fields centered $\sim 4^\circ$ from the fovea in the lower-left visual field.

Behavioral task: We trained the subject to maintain fixation on a 0.6° blue dot at the center of a flat-screen cathode ray tube monitor positioned 36 cm from its eyes. The background of the display was 50% gray. We measured the monitor luminance gamma functions using a photometer and linearized the relationship between input voltage and output luminance using lookup tables. The subject was trained to maintain fixation on the central dot for 2 seconds while no other visual stimulus was presented, at which time the fixation point was moved 11.6° in a random direction and the animal received a liquid reinforcement for making a saccade to the new location.

Microelectrode array recordings: Signals from the microelectrode arrays were band-pass filtered (0.3 - 7500 Hz), digitized at 30 kHz and amplified by a Grapevine system (Ripple). Signals crossing a threshold (periodically adjusted using a multiple of the root-mean-squared [RMS] noise for each channel) were stored for offline analysis. These waveform segments were sorted using an automated clustering algorithm [Shoham et al., 2003] followed by manual refinement using custom MATLAB software [Kelly et al., 2007] (available at http://www.smithlab.net/spikesort.html), taking into account the waveform shapes and interspike interval distributions. After sorting, we calculated the signal-to-noise (SNR) ratio of each candidate unit as the ratio of the average waveform amplitude to the standard deviation of the waveform noise [Kelly et al., 2007]. Candidates with an SNR below 2.5 were discarded. Signals were also filtered from $0.3-250$ Hz with a digital Butterworth filter and sampled at 1 kHz to provide LFPs.

LFP preprocessing: We assume that the oscillation modulating spiking activity is explicitly within the surrounding LFP. The naive way of selecting LFP is using the one recorded at the same electrode for each neuron. Since spike waveforms might contaminate the LFP spectrum [Buzsáki et al.,

2012, Ray and Maunsell, 2011], we computed LFP related to each neuron as the average of LFPs recorded on its neighboring electrodes. Another way of avoiding spike bleed-through is to choose the LFP on any electrodes adjacent to the neuron. In S2 Fig. AB, we show that LFPs selected by all three methods are very similar. We also computed the spike-triggered average (STA) field potential using these three different methods. Their shapes are almost the same (S2 Fig. CD). We then bandpass filtered the LFP using Chebyshev type II filter design with passband $4-25$ Hz. After we got the filtered oscillatory signal (Fig. 5BE), we applied the Hilbert transform to estimate the instantaneous phase for further model fitting [Jia et al., 2013].

6 Results

6.1 Point process model for spike trains

We assume that the spiking of each neuron follows a point process and, following [Kass et al., 2014] (page 592), we write its conditional intensity function as $\lambda(t|H_t, X_t)$, where H_t represents the spike history (auto-history), and the covariate X_t represents other external factors. In this work, we let X_t include the stimulus and the LFP phase, denoted by $X_t = (S_t, \Phi_t)$. The complete model has been described as Eq.(9) in Methods 5.2.

We use splines to capture stimulus and auto-history effects, and circular splines to capture LFP phase effects (See Appendix 10.1). Our point process model thus takes the form of a standard generalized linear model (GLM). We also ensure identifiability by imposing a set of restrictions (Equations (18) and (19)), which are implemented within a maximum likelihood estimation (MLE) algorithm (See Appendix 10.2). The parametric bootstrap is used for acquiring 95% confidence bands.

To illustrate the ability of the MLE algorithm to recover the model in Equation (9), we simulated 100 spike trains (Fig. 1A) with known functions $\lambda_1(t)$, $\lambda_2(t - t^*)$ and $\lambda_3(\phi)$. Using the simulated spike trains and phase of the oscillatory drive (representing a network-wide oscillation), the MLE algorithm accurately fit the underlying spike history (Fig. 1B), stimulus (Fig. 1C) and phase modulation (Fig. 1D) effects. Our approach can thus accurately recover the statistical relationships between firing rate and various external factors.

6.2 Synchrony and Oscillatory Phase

We now use point process regression of our GLMs (9) and (10) to analyze the contribution of network-wide oscillations to the synchronous spiking of two neurons. We first present numerical simulation results where ground truth is known and then apply the same technique to experimental neural recordings.

In the Introduction, we described how GLMs can be used to assess the role of some potentially relevant factors in modulating spike synchrony. We designed a scenario in which we tested the contribution of a network-wide oscillation (i.e., an oscillatory LFP) to the number of synchronous spikes observed. This scenario is illustrated schematically in Fig. 2 for two neurons. The stimulus effects (i.e., the tuning) of the two neurons are different, and both neurons' spiking activities are influenced by their own recent spike histories. Critically, these two neurons also receive a common oscillatory signal with phase Φ_t that modulates their firing rate, but their individual phase modulation curves are shifted (i.e., they have different preferred phases Φ_{pref}). Because the preferred phase modulates the average timing of each spike in one oscillatory cycle (in this example, $\sim$10 ms), differences in preferred phase lead to a relative shift in spike timing between the two neurons. The larger this shift, the less synchronized are their spikes. As a result, the observed number of synchronized spikes is dependent on the difference of preferred phase $\Delta\Phi_{pref}$.

This simple scenario was used to demonstrate the effectiveness of the procedure, in principle, and to investigate its statistical power. The assumption that two neurons have different phase modulation curves has been reported both experimentally [Jia et al., 2013, Snyder and Smith, 2015] and theoretically [Richardson, 2008]. Jia et al. [Jia et al., 2013] have shown that neurons in area

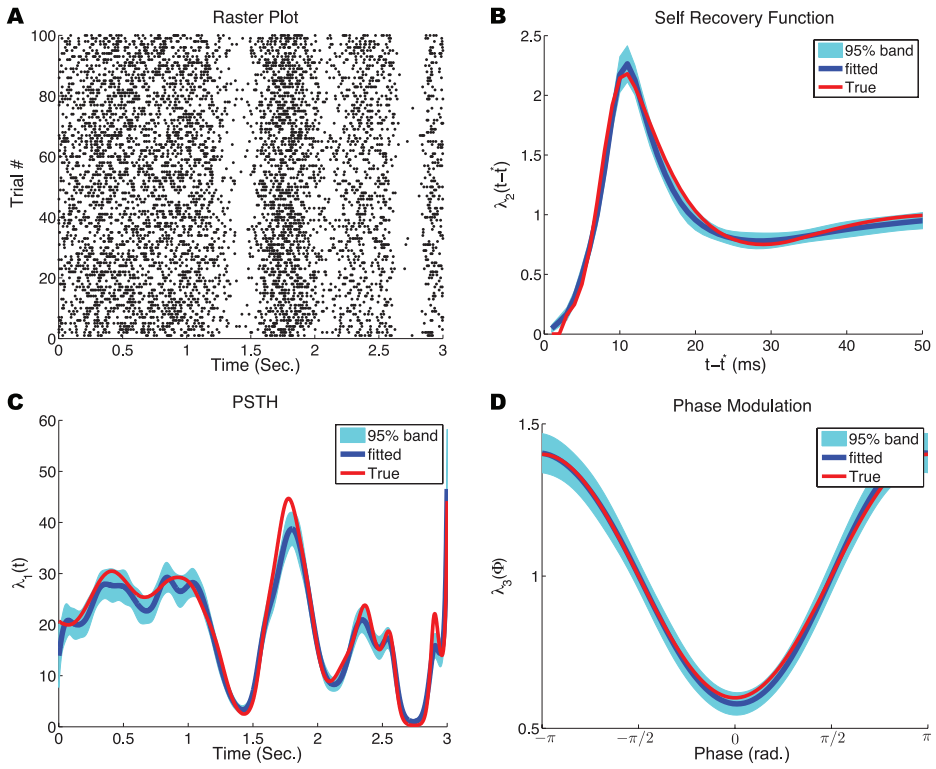

Figure 1: **Simulated spike trains and results of model fitting.** (A) Simulated spike trains in response to a fluctuating stimulus and oscillatory drive. (B,C,D) Ground truth (red) and fitted results (blue) for different terms in the firing-rate probability model. For each fitted result, we used a parametric bootstrap to determine the 95% confidence band (cyan). (B) Effect of auto-history $\lambda_2(t - t^*)$ on output firing rate. (C) Effect of stimulus $\lambda_1(t)$ on output firing rate. (D) Phase modulation curve $\lambda_3(\phi)$ of firing rate.

V1 have various preferred phases and the distribution of the preferred phase can change in response to different stimuli. Richardson [Richardson, 2008] computed analytically the modulation of the oscillatory signal for an exponential integrated-and-fire neuron. He showed that the modulation is influenced by biophysical properties of the neuron. He also showed that there is a phase lag between the peak firing rate and the peak of the oscillatory signal, which corresponds to the preferred phase in $\lambda_3(\phi)$, and this phase lag is dependent on properties of the neuron. Usually the oscillations near two neurons in a small area are very similar; thus the assumption that two neurons receive a common modulation is reasonable. For two neurons located far apart (e.g., two brain areas), this assumption should be useful as long as the two oscillations are coherent. This more general case is relevant to hypotheses about mechanisms of neural communication [Fries, 2005, Jia et al., 2013].

To demonstrate directly the relationship between an oscillatory LFP and spike synchrony, we simulated spike trains from two neurons, then fitted models (9) and (10). For each model we used the estimator

$$\hat{\zeta}_{12} = \frac{\text{Observed number of synchronized spikes}}{\text{Predicted number of synchronized spikes}} = \frac{N_{obs}}{N_{pred}}$$

of its theoretical counterpart ζ_{12} defined in [Kelly and Kass, 2012] (See Methods 5.3). Under conditional independence, we have $\log \zeta_{12} = 0$, while conditional dependence yields either excess synchrony ($\log \zeta_{12} > 0$) or suppressed synchrony ($\log \zeta_{12} < 0$). We tested $H_0 : \log \zeta_{12} = 0$ using a parametric bootstrap (see Appendix 10.3). Results are shown in Fig. 3. Using model (10) (i.e., without the oscillatory factor) we found that $\log \hat{\zeta}_{12}$ is dependent on $\Delta\Phi_{pref}$. This is because the

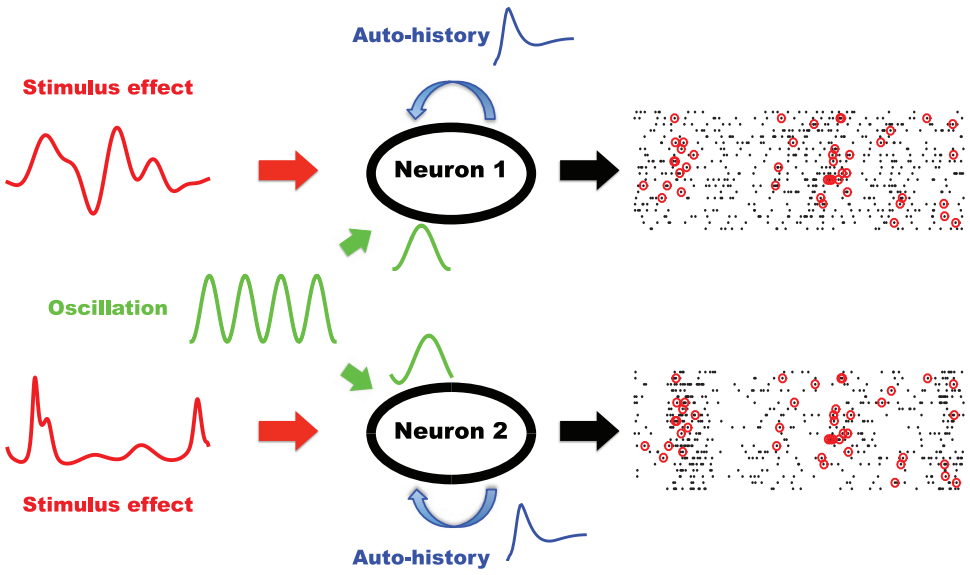

Figure 2: **Schematic illustration of the contribution of a network-wide oscillation to synchronous spiking between two neurons.** The firing probability of each neuron is influenced by three factors: stimulus, auto-history and an oscillatory drive. The oscillatory drive is shared by the two neurons, but each neuron exhibits a unique phase modulation curve. Spike trains of the two neurons are observed and synchronized spikes are counted (red circles).

relative phase preference of the two neurons changed the observed number of synchronized spikes, while the predicted number is almost the same when the contribution of the oscillatory LFP is disregarded. In contrast, when we included the oscillatory factor according to Equation (9), we found $\log \hat{\zeta}_{12}$ to be close to 0 and independent of $\Delta\Phi_{pref}$. Thus, including the oscillatory factor in our model removes the apparent conditional dependence of the predicted spike synchrony on the relative phase preference of the two neurons, and we can conclude that spike synchrony is associated with the oscillatory phase.

We picked two different values of $\Delta\Phi_{pref}$ (purple and cyan arrows in the Fig. 3A) to demonstrate the described hypothesis test. In the first example, we obtained evidence against the null hypothesis of $\log \zeta_{12} = 0$ using the simplified model (Fig. 3B). That is, there is evidence that the two neurons are not conditionally independent given only the stimulus effects and spike history effects: they exhibit significant levels of excess spike synchrony. Fig. 3C shows that including the oscillatory factor accounts for this excess synchrony. In other words, consideration of the oscillatory LFP can explain the higher than expected levels of spike synchrony predicted by the stimulus and spike history effects alone. In turn, lower than expected levels of spike synchrony predicted by the stimulus and spike history effects alone can be explained by consideration of the oscillatory LFP in the second example, in which the oscillatory LFP suppresses spike synchrony (Fig. 3D,E).

We also investigated the amount of data needed to reliably detect excess synchrony by generating spike trains with varying numbers of trials, varying values of ζ, and two levels of firing rate, and then computing the probability of rejecting the null hypothesis (i.e., the statistical power, see Appendix 10.4). Fig. 3 F displays the power when we used the same simulation parameters (apart from ζ and number of trials) as in Fig. 3 A-E. A standard target for power in the statistics literature is 0.8, and we have indicated this level of power with a red line in Fig. 3 F. Thus, to attain this high level of power when $\zeta = 1.125$ we need 70 trials, but when $\zeta = 1.4$ we need only 5 trials. This number is also highly dependent on the mean firing rate. When we change the firing rate from 25 Hz to 10 Hz, we need much more data to detect excess synchrony (Fig. 3G). The simulation procedure is

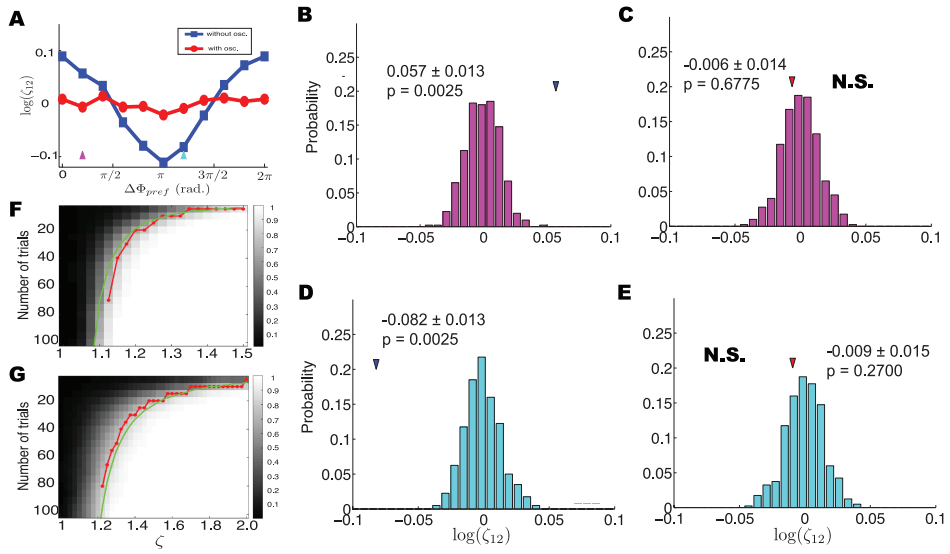

Figure 3: **Network-wide oscillations can enhance or suppress the predicted levels of spike synchrony.** (A) Dependence of $\log \hat{\zeta}_{12}$ on the difference in preferred phases between two neurons, as computed using models with and without an oscillatory factor. Purple and cyan arrows indicate two different $\Delta(\Phi_{pref})$s. (B) Bootstrap-generated distribution of $\log \hat{\zeta}_{12}$ values under the null hypothesis of $\log \zeta_{12} = 0$. Arrowhead shows the value of $\log \hat{\zeta}_{12}$ computed by the simplified model. Thus, a significantly larger number of synchronous spikes is observed than predicted by the model lacking an oscillatory factor ($\log(\hat{\zeta}_{12}) = 0.057 \pm 0.013$, p value $= 0.0025$). (C) Including an oscillatory factor in the model yields an accurate prediction of the observed number of synchronous spikes ($\log(\hat{\zeta}_{12}) = -0.006 \pm 0.014$, p value $= 0.6775$). (D, E) Same as (B,C) for different preferred phases that lead to significantly lower synchrony than predicted when an oscillatory factor is not included in the model (D: $\log(\hat{\zeta}_{12}) = -0.082 \pm 0.013$, p value $= 0.0025$; E: $\log(\hat{\zeta}_{12}) = -0.009 \pm 0.015$, p value $= 0.2700$). (F) Dependence of the power on number of trials and ζ. The mean firing rate is 25 Hz. The red and green lines indicate choices of ζ and N for which the power equals 0.8, based on simulation and theory respectively. (G) Same as (F), but the mean firing rate is 10 Hz.

computationally slow, but a fast approximation is given by

$$N = \left\lceil \frac{1}{T\lambda_1\lambda_2\delta} \left(\frac{\Phi^{-1}(0.95) - \Phi^{-1}(0.2)/\sqrt{\zeta}}{\log \zeta} \right)^2 \right\rceil$$

where T is the length of one trial, λ_1 and λ_2 are mean firing rates of two neurons, and δ is the bin size for detecting synchronized spikes. The approximate power from this formula is given by the green curves in Fig. 3F,G. The formula is derived in Appendix 10.4.

6.3 Applications to Experimental Neural Recordings

To further demonstrate the value of our approach, we next examined the relationship between an oscillatory signal and spike synchrony in experimental neural recordings from two distinct preparations: hippocampal CA1 pyramidal cells recorded *in vitro* and V4 neurons recorded *in vivo*.

6.3.1 Hippocampal CA1 pyramidal cells

We first designed an experiment to resemble the scenario proposed in Fig. 2 using whole-cell patch clamp recordings in a controllable acute slice preparation. In this experiment, we recorded the spiking response of, and spike synchrony between, two CA1 pyramidal cells (Fig. 4A,B) in response to an arbitrary stimulus with and without a shared oscillatory signal. Critically, to directly test the

relationship between the oscillatory signal and the resulting spike synchrony, we limited potential confounding influences on spike synchrony (e.g., common neuromodulatory influences, coupling between two neurons) by recording these neurons sequentially in two separate slices. Each neuron was injected with 100 trials of a 2 s-long 150 pA step current overlaid with a slow sinusoidal current (2 Hz frequency, 25 pA amplitude) and white noise ($\sigma = 10$ pA) to evoke physiological spike trains with low trial-to-trial reliability. The slow 2 Hz component was the same for all trials, and it generated visible time-varying fluctuations that are visible in the raster plots in Fig 4A,B, which led to a time-varying PSTH that was captured by the $\lambda_1(t)$ term in Equation (9). On 50 random trials ("Exp. 2"), an additional sinusoidal current (40 Hz frequency, 15 pA amplitude) with random initial phase (but identical between the two neurons) was also injected to simulate a gamma frequency network-wide oscillation. The 40 Hz component was not consistent over trials due to varying initial phases (S1 Fig. A), and its effect is, therefore, not captured by $\lambda_1(t)$. Instead, this 40 Hz modulatory effect was captured through the term $\lambda_3(\Phi_t)$ in Equation (9).

Thus, in the 50 trials without the simulated network-wide oscillation ("Exp. 1"), each neuron fired according to the its own stimulus and auto-history effects, generating a certain level of largely spontaneous spike synchrony reflecting the neurons' fluctuating stimulus-driven firing rates. Using

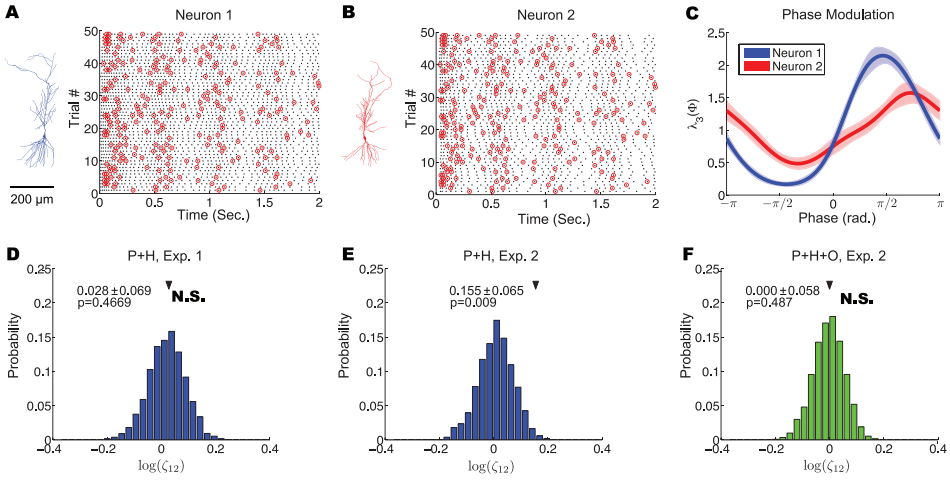

Figure 4: **Shared oscillations contribute to spike synchrony between hippocampal CA1 pyramidal cells *in vitro*.** (A, B) Reconstructed morphologies (left) and raster plots of spike trains (right) evoked in two CA1 pyramidal cells by an arbitrary stimulus waveform with a shared oscillatory signal ("Exp. 2"). Red circles show synchronized spikes between the two neurons. (C) Estimated phase modulation of the two recorded neurons in response to a shared oscillatory signal simulating a network-wide oscillation. (D) In the absence of a shared oscillatory signal, the simplified model (stimulus, or PSTH effects [P] + spike or auto-history effects [H]) lacking an oscillatory factor accurately predicts the observed number of synchronous spikes between the two neurons. (E,F) In the presence of a shared oscillatory signal, the simplified model (P+H) fails to explain the observed number of synchronous spikes (E) while the full model (stimulus, or PSTH effects [P] + spike or auto-history effects [H] + an oscillatory factor [O]) containing an oscillatory factor accurately predicts the observed number of synchronous spikes (F).

our simplified model (Equation (10)), we fit the spike trains from "Exp. 1" and predicted the number of synchronous spikes. As expected, the observed and predicted number of synchronous spikes closely matched (Fig. 4D), consistent with the two neurons being conditionally independent given the arbitrary stimulus waveform and their own recent spiking histories. That is, no other factors were necessary to explain the observed number of synchronous spikes. However, using our simplified model to fit the spike trains from "Exp. 2" (Fig. 4A,B), we observed a significantly greater number of synchronous spikes than could be explained by the stimulus and the neurons' spike histories alone (Fig. 4E). This conditional dependence between the two neurons arose because the firing of the two neurons was modulated by the simulated network-wide oscillation (Fig. 4C). Indeed, using our full model (Equation (9)) to fit the spike trains from "Exp. 2" (S1 Fig. B,C,D), the number of

synchronous spikes observed closely matched the number of synchronous spikes predicted (Fig. 4F).

This experiment demonstrates that when two experimentally recorded neurons are not modulated by a shared oscillatory signal, then the simplified model (Equation (10)) can account for the observed number of synchronous spikes. However, when two neurons are modulated by a shared oscillatory signal (such as an oscillatory LFP, reflecting a network-wide oscillation), then a model including this oscillatory factor (Equation (9)) is necessary to account for the observed number of synchronous spikes. In contrast with our simulation above, the firing of these CA1 neurons is not described by the GLM in Equation (9) exactly. This model mismatch did not restrict the application of our method.

6.3.2 V4 neurons

In this experiment, spike trains from a pair of neural units in V4 were simultaneously recorded (Fig. 5A,D) with a multi-electrode array during a fixation task in which spontaneous activity was measured. These data have been analyzed in another paper [Snyder and Smith, 2015], which examined the relationship between individual neuron's activity and large-scale network state. Here we wanted to test whether network-wide oscillations contribute to the excess pairwise synchrony. For each neuron, we defined its surrounding LFP as the average of LFPs recorded at its adjacent electrodes. The spike-triggered average of the LFP for two neurons showed that the two neurons are phase locked to their surrounding field potential (S2 Fig. CD and [Snyder and Smith, 2015]). We also found that the LFP showed a prominent slow oscillation (Fig. 5B,E). The LFP is thought to be the integrated effect of synaptic and spiking activity [Buzsáki et al., 2012] near the recording sites. We filtered the LFP on each electrode within the 4-25 Hz band and extracted its phase to fit our full model (Equation (9)). Using the same procedure as in the case of the hippocampal CA1 pyramidal cells, we found that a significantly larger number of synchronous spikes were observed than could be explained by the simplified model (Fig. 5C), while the full model fully explained the spike synchronization observed between the two neurons (Fig. 5F). These results show that for these two neurons *in vivo*, spike synchronization is associated with the network-wide oscillation.

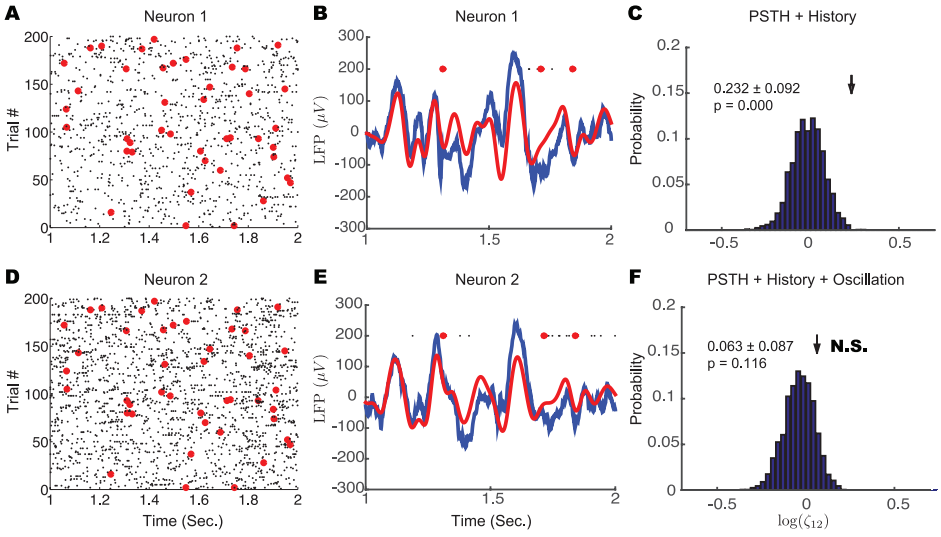

Figure 5: **Shared oscillations contribute to spike synchrony between V4 neurons *in vivo*.** (A,D) Raster plot of spike trains from two neurons recorded simultaneously. Red circles show synchronized spikes between the two neurons. (B,E) Raw (blue) and 4-25 Hz filtered (red) surrounding LFP related with each neuron for a single trial. (C,F) The simplified model failed to explain the observed number of synchronous spikes (C), while the full model containing an oscillatory factor fully accounts for the observed number of synchronous spikes.

7 Discussion

In this paper, we have shown how the GLM methods of [Lepage et al., 2011, Lepage et al., 2013, Kass et al., 2011, Kelly and Kass, 2012] may be combined in order to assess the potential contribution of network-wide oscillations to neural synchrony. The novel approach presented in this study complements existing alternatives [Grün et al., 2002, Grün, 2009, Pipa et al., 2008] by: introducing models of single neuron firing based on stimulus-related fluctuations as well as a network-wide oscillatory signal; using those models to make predictions about spike synchronization; and quantifying departures from those predictions in the observed data. We demonstrated the advantages of this novel approach using both neural simulations and experimental neural recordings *in vitro* and *in vivo*.

In our analyses, we have utilized a repeated-trial structure, which allowed us to estimate the stimulus effects as a function of time, $\lambda_1(t)$. We note, however, that the same approach could be applied using a linear response filter [Kelly et al., 2010, Park et al., 2014, Pillow et al., 2008] or analogous nonlinear methods. Previous work has shown the close relationship between GLM neurons and integrate-and-fire neurons [Koyama and Kass, 2008, Ostojic and Brunel, 2011, Paninski et al., 2010]. We only considered one band of oscillation in simulation and experimental examples, but it is straightforward to extend this method to the case of multiple oscillations by including additional terms in the model of Equation (9). Sometimes the firing probability may be related to the amplitude of the oscillation A_t, or the magnitude of an LFP B_t (cf. [Lepage et al., 2013]). If so, we can change $f_3(\Phi_t)$ to $f_3(A_t)$ or $f_3(B_t)$. Overall, the key step of this method is to build an approximately correct GLM. The specific form of GLM depends on the data and we can check model performance using time rescaling [Brown et al., 2002]. We have also included a simulation to show that even when the model is mis-specified, and therefore less sensitive, it can detect spike-LFP relationships (S3 Fig.). We have also defined spike synchrony to involve the firing of two neurons within a few milliseconds of each other (i.e., with zero lag on average). In other contexts, however, interest may focus on two neurons firing in procession with a consistent positive or negative lag of many milliseconds. Our approach could be easily applied to such lagged-synchrony cases as well.

In this paper, we consider only pairwise synchrony. By combining our approach with the procedure proposed by [Kelly and Kass, 2012], we can also test the role of oscillations in three-way synchrony. Briefly, we fit all single neuron firing probabilities and then compute the pairwise synchrony coefficients $\hat{\zeta}_{ij}$; we can then use an iterative algorithm to estimate the three-way synchrony coefficient $\hat{\zeta}_{ijk}$, and to test the null hypothesis of two-way interactions, instead of three-way interaction. In principle the same steps may be followed for more than three neurons, but simulations in [Kelly and Kass, 2012] show that very large data sets would be needed in order to demonstrate higher-order interactions convincingly in the absence of stronger assumptions about the nature of those interactions.

8 Conclusion

It has been argued that synchronous firing resulting from network-wide oscillations could provide an essential mechanism of network information flow, and further serve as a a marker distinguishing normal from diseased states (e.g., see [Bosman et al., 2012, Buzsáki and Draguhn, 2004, Grothe et al., 2012, Joshua et al., 2009, Ratté et al., 2013, Singer, 1999, Uhlhaas and Singer, 2010, Womelsdorf and Fries, 2007]). On the other hand, there has been considerable debate on this subject (see [Stanley, 2013] and references therein). We remain agnostic on this, and importantly, the value of our methods does not depend on the ultimate outcome of this debate. Instead, we view synchrony, more descriptively, as a feature of spike train data that needs to be explained. To this end, the framework that we have introduced here is useful for quantifying the extent to which oscillations, as a feature of neural activity, are associated with synchronous spiking among neurons. Armed with this method, future experiments can measure oscillations and synchrony in a statistical framework in which their contributions to cognitive and behavioral processes can be accurately quantified.

9 Acknowledgments

This work was supported by National Institute of Mental Health (NIMH, R01MH064537), Richard King Mellon Foundation (Presidential Fellowship in Life Sciences), and National Institute on Drug Abuse (NIDA, R90DA023426), Pennsylvania Department of Health (Formula SAP4100054842); I thank my collaborators Shawn Burton, Adam Snyder, Matthew Smith, and Nathaniel Urban for their great work in experimental data collection; I would like to give my special thanks to my advisor Robert Kass for his supervision in this project.

References

[Bosman et al., 2012] Bosman, C. A., Schoffelen, J. M., Brunet, N., Oostenveld, R., Bastos, A. M., Womelsdorf, T., Rubehn, B., Stieglitz, T., De Weerd, P., and Fries, P. (2012). Attentional Stimulus Selection through Selective Synchronization between Monkey Visual Areas. *Neuron*, 75:875–888.

[Brette, 2012] Brette, R. (2012). Computing with neural synchrony. *PLoS Computational Biology*, 8.

[Brown et al., 2002] Brown, E. N., Barbieri, R., Ventura, V., Kass, R. E., and Frank, L. M. (2002). The time-rescaling theorem and its application to neural spike train data analysis. *Neural Computation*, 14(2):325–346.

[Burton and Urban, 2014] Burton, S. D. and Urban, N. N. (2014). Greater excitability and firing irregularity of tufted cells underlies distinct afferent-evoked activity of olfactory bulb mitral and tufted cells. *The Journal of Physiology*, 00:1–22.

[Buzsáki et al., 2012] Buzsáki, G., Anastassiou, C. A., and Koch, C. (2012). The origin of extracellular fields and currents — EEG, ECoG, LFP and spikes. *Nature Reviews Neuroscience*, 13(6):407–420.

[Buzsáki and Draguhn, 2004] Buzsáki, G. and Draguhn, A. (2004). Neuronal oscillations in cortical networks. *science*, 304(5679):1926–1929.

[Colgin et al., 2009] Colgin, L. L., Denninger, T., Fyhn, M., Hafting, T., Bonnevie, T., Jensen, O., Moser, M.-B., and Moser, E. I. (2009). Frequency of gamma oscillations routes flow of information in the hippocampus. *Nature*, 462(7271):353–7.

[Denker et al., 2011] Denker, M., Roux, S., Linden, H., Diesmann, M., Riehle, A., and Grun, S. (2011). The Local Field Potential Reflects Surplus Spike Synchrony. *Cerebral Cortex*, 21(12):2681–2695.

[Engel et al., 2001] Engel, A. K., Fries, P., and Singer, W. (2001). Dynamic predictions: oscillations and synchrony in top-down processing. *Nature Reviews Neuroscience*, 2:704–716.

[Feng et al., 2000] Feng, G., Mellor, R. H., Bernstein, M., Keller-Peck, C., Nguyen, Q. T., Wallace, M., Nerbonne, J. M., Lichtman, J. W., and Sanes, J. R. (2000). Imaging neuronal subsets in transgenic mice expressing multiple spectral variants of GFP. *Neuron*, 28:41–51.

[Friedrich et al., 2004] Friedrich, R. W., Habermann, C. J., and Laurent, G. (2004). Multiplexing using synchrony in the zebrafish olfactory bulb. *Nature Neuroscience*, 7(8):862–871.

[Fries, 2005] Fries, P. (2005). A mechanism for cognitive dynamics: Neuronal communication through neuronal coherence. *Trends in Cognitive Sciences*, 9:474–480.

[Geman, 2006] Geman, S. (2006). Invariance and selectivity in the ventral visual pathway. *Journal of Physiology Paris*, 100:212–224.

[Graves et al., 2009] Graves, S., Hooker, G., and Ramsay, J. (2009). *Functional data analysis with R and MATLAB*. Springer, New York.

[Gregoriou et al., 2009] Gregoriou, G. G., Gotts, S. J., Zhou, H., and Desimone, R. (2009). High-frequency, long-range coupling between prefrontal and visual cortex during attention. *Science*, 324:1207–1210.

[Grothe et al., 2012] Grothe, I., Neitzel, S. D., Mandon, S., and Kreiter, A. K. (2012). Switching neuronal inputs by differential modulations of gamma-band phase-coherence. *The Journal of Neuroscience*, 32(46):16172–80.

[Grün, 2009] Grün, S. (2009). Data-driven significance estimation for precise spike correlation. *Journal of Neurophysiology*, 101(January 2009):1126–1140.

[Grün et al., 2002] Grün, S., Diesmann, M., and Aertsen, A. (2002). Unitary events in multiple single-neuron spiking activity: II. Nonstationary data. *Neural Computation*, 14:81–119.

[Jia et al., 2013] Jia, X., Tanabe, S., and Kohn, A. (2013). Gamma and the Coordination of Spiking Activity in Early Visual Cortex. *Neuron*, 77(4):762–74.

[Joshua et al., 2009] Joshua, M., Adler, A., Prut, Y., Vaadia, E., Wickens, J. R., and Bergman, H. (2009). Synchronization of Midbrain Dopaminergic Neurons Is Enhanced by Rewarding Events. *Neuron*, 62:695–704.

[Kass and Ventura, 2001] Kass, R. and Ventura, V. (2001). A spike-train probability model. *Neural Computation*, 1720:1713–1720.

[Kass et al., 2014] Kass, R. E., Eden, U. T., and Brown, E. N. (2014). *Analysis of Neural Data*. Springer Series in Statistics.

[Kass et al., 2011] Kass, R. E., Kelly, R. C., and Loh, W.-L. (2011). Assessment of Synchrony in Multiple Neural Spike Trains Using Loglinear Point Process Models. *The Annals of Applied Statistics*, 5(2B):1262–1292.

[Kaufman et al., 2005] Kaufman, C. G., Ventura, V., and Kass, R. E. (2005). Spline-based non-parametric regression for periodic functions and its application to directional tuning of neurons. *Statistics in Medicine*, 24(14):2255–65.

[Kelly and Kass, 2012] Kelly, R. C. and Kass, R. E. (2012). A framework for evaluating pairwise and multiway synchrony among stimulus-driven neurons. *Neural Computation*, 24(8):2007–32.

[Kelly et al., 2010] Kelly, R. C., Kass, R. E., Smith, M. a., and Lee, T. S. (2010). Accounting for network effects in neuronal responses using L1 regularized point process models. *Advances in Neural Information Processing Systems*, 23(2):1099–1107.

[Kelly et al., 2007] Kelly, R. C., Smith, M. A., Samonds, J. M., Kohn, A., Bonds, A. B., Movshon, J. A., and Lee, T. S. (2007). Comparison of recordings from microelectrode arrays and single electrodes in the visual cortex. *The Journal of Neuroscience*, 27:261–264.

[Koyama and Kass, 2008] Koyama, S. and Kass, R. E. (2008). Spike train probability models for stimulus-driven leaky integrate-and-fire neurons. *Neural Computation*, 20(7):1776–1795.

[Lepage et al., 2013] Lepage, K. Q., Gregoriou, G. G., Kramer, M. a., Aoi, M., Gotts, S. J., Eden, U. T., and Desimone, R. (2013). A procedure for testing across-condition rhythmic spike-field association change. *Journal of Neuroscience Methods*, 213(1):43–62.

[Lepage et al., 2011] Lepage, K. Q., Kramer, M. A., and Eden, U. T. (2011). The dependence of spike field coherence on expected intensity. *Neural Computation*, 23(9):2209–41.

[Mizuseki and Buzsaki, 2014] Mizuseki, K. and Buzsaki, G. (2014). Theta oscillations decrease spike synchrony in the hippocampus and entorhinal cortex. *Philosophical transactions of the Royal Society of London. Series B, Biological sciences*, 369:20120530.

[Niebur et al., 2002] Niebur, E., Hsiao, S. S., and Johnson, K. O. (2002). Synchrony: A neuronal mechanism for attentional selection? *Current Opinion in Neurobiology*, 12:190–194.

[Ostojic and Brunel, 2011] Ostojic, S. and Brunel, N. (2011). From spiking neuron models to linear-nonlinear models. *PLoS Computational Biology*, 7(1):e1001056.

[Paninski et al., 2010] Paninski, L., Brown, E. N., Iyengar, S., and Kass, R. E. (2010). Statistical models of spike trains. In Laing, C. and Lord, G. J., editors, *Stochastic Methods in Neuroscience*, pages 272–296. Oxford University Press.

[Park et al., 2014] Park, I. M., Meister, M. L. R., Huk, A. C., and Pillow, J. W. (2014). Encoding and decoding in parietal cortex during sensorimotor decision-making. *Nature Neuroscience*, 17(10):1395–1403.

[Pillow et al., 2008] Pillow, J. W., Shlens, J., Paninski, L., Sher, A., Litke, A. M., Chichilnisky, E. J., and Simoncelli, E. P. (2008). Spatio-temporal correlations and visual signalling in a complete neuronal population. *Nature*, 454(7207):995–9.

[Pipa et al., 2008] Pipa, G., Wheeler, D. W., Singer, W., and Nikolić, D. (2008). NeuroXidence: Reliable and efficient analysis of an excess or deficiency of joint-spike events. *Journal of Computational Neuroscience*, 25:64–88.

[Ratté et al., 2013] Ratté, S., Hong, S., De Schutter, E., and Prescott, S. A. (2013). Impact of neuronal properties on network coding: roles of spike initiation dynamics and robust synchrony transfer. *Neuron*, 78(5):758–72.

[Ray and Maunsell, 2011] Ray, S. and Maunsell, J. H. R. (2011). Different origins of gamma rhythm and high-gamma activity in macaque visual cortex. *PLoS Biology*, 9(4).

[Richardson, 2008] Richardson, M. J. E. (2008). Spike-train spectra and network response functions for non-linear integrate-and-fire neurons. *Biological Cybernetics*, 99(4-5):381–92.

[Robbe et al., 2006] Robbe, D., Montgomery, S. M., Thome, A., Rueda-Orozco, P. E., McNaughton, B. L., and Buzsaki, G. (2006). Cannabinoids reveal importance of spike timing coordination in hippocampal function. *Nature Neuroscience*, 9(12):1526–1533.

[Salinas and Sejnowski, 2001] Salinas, E. and Sejnowski, T. J. (2001). Correlated neuronal activity and the flow of neural information. *Nature Reviews Neuroscience*, 2:539–550.

[Sejnowski and Paulsen, 2006] Sejnowski, T. J. and Paulsen, O. (2006). Network oscillations: emerging computational principles. *The Journal of Neuroscience*, 26(6):1673–1676.

[Shoham et al., 2003] Shoham, S., Fellows, M. R., and Normann, R. A. (2003). Robust, automatic spike sorting using mixtures of multivariate t-distributions. *Journal of Neuroscience Methods*, 127(2):111–122.

[Siapas et al., 2005] Siapas, A. G., Lubenov, E. V., and Wilson, M. A. (2005). Prefrontal phase locking to hippocampal theta oscillations. *Neuron*, 46(1):141–51.

[Singer, 1999] Singer, W. (1999). Neuronal synchrony: a versatile code for the definition of relations? *Neuron*, 24(1):49–65.

[Sirota et al., 2008] Sirota, A., Montgomery, S., Fujisawa, S., Isomura, Y., Zugaro, M., and Buzsáki, G. (2008). Entrainment of neocortical neurons and gamma oscillations by the hippocampal theta rhythm. *Neuron*, 60(4):683–97.

[Smith and Sommer, 2013] Smith, M. A. and Sommer, M. A. (2013). Spatial and temporal scales of neuronal correlation in visual area V4. *The Journal of Neuroscience*, 33:5422–32.

[Snyder et al., 2015] Snyder, A. C., Morais, M. J., Willis, C. M., and Smith, M. A. (2015). Global network influences on local functional connectivity. *Nature Neuroscience*, 18(5):736–743.

[Snyder and Smith, 2015] Snyder, A. C. and Smith, M. A. (2015). Stimulus-dependent spiking relationships with the EEG. *Journal of Neurophysiology*.

[Stanley, 2013] Stanley, G. B. (2013). Reading and writing the neural code. *Nature Neuroscience*, 16:259–63.

[Tiesinga et al., 2008] Tiesinga, P., Fellous, J.-M., and Sejnowski, T. J. (2008). Regulation of spike timing in visual cortical circuits. *Nature Reviews Neuroscience*, 9:97–107.

[Uhlhaas and Singer, 2010] Uhlhaas, P. J. and Singer, W. (2010). Abnormal neural oscillations and synchrony in schizophrenia. *Nature Reviews Neuroscience*, 11(2):100–13.

[Womelsdorf and Fries, 2007] Womelsdorf, T. and Fries, P. (2007). The role of neuronal synchronization in selective attention. *Current Opinion in Neurobiology*, 17:154–160.

10 Appendix

10.1 Approximate Function with Spline Basis

To fit the smooth functions $f_1(\cdot), f_2(\cdot)$ and $f_3(\cdot)$ we use cubic splines of the form

$$\log\left(\lambda(t|H_t, X_t)\right) = \sum_i a_i(t)\alpha_i + \sum_j b_j(t - t^*) \cdot \beta_j + \sum_k r_k(\Phi_t) \cdot \gamma_k \tag{13}$$

where $\{a_i(t)\}$ is a B-spline basis set for $f_1(t)$ within the range $t \in (0, T]$, $\{b_j(t - u_t^*)\}$ is a B-spline basis set for $f_2(t - t^*)$, and $\{r_k(\phi)\}$ is circular spline basis set for $f_3(\Phi_t)$. Thus, we use maximum likelihood to fit the coefficients $\mathbf{\Theta} = \{\alpha, \beta, \gamma\}$. We used open source software FDAfuns [Graves et al., 2009] to create each B-spline basis sets after manually selecting knots. For the circular spline

we pick knots equally spaced in $[-\pi, \pi]$. Once we get all knots $\{\phi_i\}$, acquiring the related basis function is straightforward [Kaufman et al., 2005] using

$$r_k(\phi) = \sum_{m=1}^{\infty} \frac{2}{(2\pi m)^4} \cos\left(2\pi m \left(\phi - \phi_k\right)\right). \tag{14}$$

In numerical implementations, we usually cut the summation from $m = 1$ to $m = 4$ because amplitude of each term decreases quickly.

10.2 Maximum Likelihood via Iteratively Re-Weighted Least Squares

Because L in equation (5) is a concave function, we can use iteratively reweighted least squares (IRLS), as in typical GLM implementations. From Equations (3), (5), and (13), we can rewrite loglikelihood in matrix form

$$L = Y^T \cdot \log \mu - I_{1\times K} \cdot \mu \tag{15}$$
$$\log \mu = \left[A \cdot \alpha + B \cdot \beta + R \cdot \gamma\right] \Delta \tag{16}$$

Here we have three parameter sets to fit $\{\alpha, \beta, \gamma\}$. If we fit all three parameter sets together, the dimension space of this GLM model is relative large. To make model fitting efficient, we prefer back-fitting, i.e., fitting each parameter set separately, and iterating cyclically. For example, when we fit the parameters $\{\alpha\}$, we hold the parameters $\{\beta, \gamma\}$ constant and rewrite Equation (16) as

$$\log \mu = V \cdot \theta + \log \mu_t^0 \tag{17}$$

where $\theta \in \{\alpha, \beta, \gamma\}$ and V is the corresponding covariate matrix. We fit $\{\alpha, \beta, \gamma\}$ in a sequence and then iterate the loop until convergence. We also must place identifiability restrictions on $\{\beta, \gamma\}$ because both the auto-history and oscillatory effects modulate the spike trains and the parameters must be constrained to provide unique solutions. We use the constraints

$$\frac{\int_0^T \exp\left[\sum_j b_j(\tau) \cdot \beta_j\right] d\tau}{T} = 1 \tag{18}$$
$$\frac{\int_{-\pi}^{\pi} \exp\left[\sum_k r_k\left(\Phi\right) \gamma_k\right] d\Phi}{2\pi} = 1. \tag{19}$$

To avoid over-fitting of the model, we also add an l_2 penalty into the objective function. Now the problem becomes minimizing objective function

$$Q = -L + \frac{\lambda}{2}|\Theta|_2 = -Y^T \cdot (V \cdot \Theta + \log \mu_t^0) + I_{1\times K} \cdot \exp(V \cdot \Theta + \log \mu_t^0) + \frac{\lambda}{2} \cdot \Theta^T \Theta. \tag{20}$$

Because the objective function Q is convex, we can iteratively maximize Θ by following the updating rule

$$\Theta^{i+1} = \Theta^i - H^{-1} \cdot \nabla Q \tag{21}$$

where H is the Hessian of Q and ∇Q is the gradient of the function, which are obtained as

$$\nabla Q = V^T \left[\exp(V \cdot \Theta + \log \mu_t^0) - Y\right] + \lambda\Theta \tag{22}$$
$$H = V^T \cdot W \cdot V + \lambda \tag{23}$$

where W is a diagonal matrix

$$W_{i,j} = \begin{cases} \exp\left(V \cdot \Theta + \log \mu_t^0\right)_i & \text{if } i = j \\ 0 & \text{otherwise.} \end{cases} \tag{24}$$

The algorithm is summarized as **Algorithm 1**, shown below.

Data: $Y, V, \Theta_0, \log \mu_t^0, \lambda$
Result: $\Theta^* = \text{argmin}_\Theta Q(\Theta)$
begin
  $Q_1 \leftarrow Q(\Theta_0)$;
  repeat
    $Q_0 \leftarrow Q_1$;
    $\nabla Q \leftarrow V^T \left[\exp(V \cdot \Theta_0 + \log \mu_t^0) - Y\right] + \lambda \Theta_0$;
    $W \leftarrow \text{diag}\left\{\exp(V \cdot \Theta_0 + \log \mu_t^0)\right\}$;
    $H \leftarrow V^T \cdot W \cdot V + \lambda$;
    $\Theta_1 \leftarrow \Theta_0 - H^{-1} \cdot \nabla Q$;
    $Q_1 \leftarrow Q(\Theta_1)$;
    $\Theta_0 \leftarrow \Theta_1$;
  until $|Q_1 - Q_0| \leq \delta$;
  return Θ_1;
end

Algorithm 1: IRLS method for finding $\text{argmin}_\Theta Q(\Theta)$

10.3 Parametric bootstrap for testing null hypothesis $H_0 : \log \zeta = 0$

Once we have $\log \hat{\zeta}$, we also need to determine its standard error and confidence interval. Furthermore, a p value is required to test the hypothesis $\log \hat{\zeta} = 0$. We use a parametric bootstrap method for these purposes, as in [Kelly and Kass, 2012]. For example, given $\hat{\lambda}_1(t|H_t, X_t)$ and $\hat{\lambda}_2(t|H_t, X_t)$ we can obtain the p value as follows:

- For i in $1 : G$ do
  1. Simulate each of the two sets of spike trains, across the same number of trials as in the data, using the respective spike train models with $\hat{\lambda}_1$ and $\hat{\lambda}_2$.
  2. Compute $\log \zeta_i$ from the spike trains generated in step 1.
- Compute the number of values $\{\log \zeta_i\}$ (out of a total of G such values) for which $|\{\log \zeta_i\}| > |\log \hat{\zeta}|$ and divide by G. This is the p value.

10.4 Power analysis

Statistical power is the probability of correctly rejecting the null hypothesis when it is false. We used the GLM model in Equation (9) to study power as a function of ζ and N (N being the number of trials). We simulated N trials of spike train data for each of two neurons, independently, using Equation (9) with intensity functions $\lambda^{(1)}(t|H_t, X_t)$ for the first neuron and $\lambda^{(2)}(t|H_t, X_t)$ for the second. The synchronous spikes in the resulting spike trains occur with probability corresponding to $\zeta = 1$ (independence). In order to obtain sets of spike trains for other values of ζ we removed all the synchronous spikes from the N simulated spike trains and replaced them with synchronous spikes generated from an intensity function $\zeta \cdot \lambda_1(t|H_t, X_t) \cdot \lambda_2(t|H_t, X_t)$, i.e., for each time bin of width δ, synchronous spikes occurred with probability $\zeta \cdot \lambda_1(t|H_t, X_t) \cdot \lambda_2(t|H_t, X_t)\delta^2$. However, while this is the desired probability of synchronous spikes, it leaves the wrong marginal probability of spiking for each neuron. To adjust these we consider the spike trains made up of only the non-synchronous spikes, and we thin these with probabilities $p^{(j)}(t)$ given by

$$p^{(j)}(t) = \frac{\lambda^{(j)}(t|H_t, X_t) - \zeta \cdot \lambda^{(1)}(t|H_t, X_t) \cdot \lambda^{(2)}(t|H_t, X_t)\,\delta}{\lambda^{(j)}(t|H_t, X_t) - \lambda^{(1)}(t|H_t, X_t) \cdot \lambda^{(2)}(t|H_t, X_t)\,\delta}$$

for $j = 1, 2$. Note that when we multiply the numerator and denominator of this expression by δ we have the ratio of the desired probability of a non-synchronous spike to the probability of a non-synchronous spike under independence (the latter probability corresponding to the process we are thinning). After obtaining all N trials we then fitted the model to these simulated spike trains, found the estimate $\hat{\zeta}$, and applied the hypothesis test using the bootstrap method. This procedure was

carried out for each ζ and N in our simulation.
Because the simulation is computationally time-consuming, for the benefit of any future efforts along these lines, we also derived a formula to approximate the number of trials needed to get 0.8 power. Suppose we have N trials, each trial is T seconds, the bin size for synchrony detection is δ. Denote the instantaneous firing rates for two neurons on trial i by $\lambda_{t,i}^{(1)}$ and $\lambda_{t,i}^{(2)}$. The number of synchronized spikes within the tth bin is $y_{t,i}^{(12)}$ and $y_{t,i}^{(12)} \sim \text{Poisson}\left(\zeta \cdot \lambda_{t,i}^{(1)} \lambda_{t,i}^{(2)} \cdot \delta^2\right)$, where ζ is the synchrony coefficient. The total number of observed synchronized spikes given $\lambda_{t,i}^{(1)}$ and $\lambda_{t,i}^{(2)}$ is $N_{obs}|\lambda_{t,i}^{(1)}, \lambda_{t,i}^{(2)} = \sum_{i=1}^{N} \sum_{t=1}^{T/\delta} y_{t,i}^{(12)}$. Then we compute $\hat{\zeta}$ conditioned on $\lambda_{t,i}^{(1)}$ and $\lambda_{t,i}^{(2)}$,

$$\hat{\zeta}|\lambda_{t,i}^{(1)}, \lambda_{t,i}^{(2)} = \frac{N_{obs}|\lambda_{t,i}^{(1)}, \lambda_{t,i}^{(2)}}{N_{pred}} = \frac{\sum_{i=1}^{N} \sum_{t=1}^{T/\delta} y_{t,i}^{(12)}}{\sum_{i=1}^{N} \sum_{t=1}^{T/\delta} \lambda_{t,i}^{(1)} \lambda_{t,i}^{(2)} \cdot \delta^2}.$$

Since $y_{t,i}^{(12)} \sim \text{Poisson}\left(\zeta \cdot \lambda_{t,i}^{(1)} \cdot \lambda_{t,i}^{(2)} \delta^2\right)$, we can easily get

$$\begin{aligned}
E\left[\hat{\zeta}|\lambda_{t,i}^{(1)}, \lambda_{t,i}^{(2)}\right] =& \frac{E\left[\sum_{i=1}^{N} \sum_{t=1}^{T/\delta} y_{t,i}^{(12)}\right]}{\sum_{i=1}^{N} \sum_{t=1}^{T/\delta} \lambda_{t,i}^{(1)} \lambda_{t,i}^{(2)} \cdot \delta^2} = \frac{\sum_{i=1}^{N} \sum_{t=1}^{T/\delta} \zeta \cdot \lambda_{t,i}^{(1)} \lambda_{t,i}^{(2)} \delta^2}{\sum_{i=1}^{N} \sum_{t=1}^{T/\delta} \lambda_{t,i}^{(1)} \lambda_{t,i}^{(2)} \cdot \delta^2} = \zeta \\
Var\left(\hat{\zeta}|\lambda_{t,i}^{(1)}, \lambda_{t,i}^{(2)}\right) =& \frac{Var\left(\sum_{i=1}^{N} \sum_{t=1}^{T/\delta} y_{t,i}^{(12)}\right)}{\left(\sum_{i=1}^{N} \sum_{t=1}^{T/\delta} \lambda_{t,i}^{(1)} \lambda_{t,i}^{(2)} \delta^2\right)^2} = \frac{\sum_{i=1}^{N} \sum_{t=1}^{T/\delta} \zeta \cdot \lambda_{t,i}^{(1)} \lambda_{t,i}^{(2)} \delta^2}{\left(\sum_{i=1}^{N} \sum_{t=1}^{T/\delta} \lambda_{t,i}^{(1)} \lambda_{t,i}^{(2)} \delta^2\right)^2} \\
=& \frac{\zeta}{\sum_{i=1}^{N} \sum_{t=1}^{T/\delta} \lambda_{t,i}^{(1)} \lambda_{t,i}^{(2)} \delta^2}.
\end{aligned}$$

Assuming $\lambda_{t,i}^{(1)}$ and $\lambda_{t,i}^{(2)}$ are independent, we have

$$E\left[\sum_{i=1}^{N} \sum_{t=1}^{T/\delta} \lambda_{t,i}^{(1)} \lambda_{t,i}^{(2)} \delta^2\right] = \sum_{i=1}^{N} \sum_{t=1}^{T/\delta} E\left[\lambda_{t,i}^{(1)}\right] E\left[\lambda_{t,i}^{(2)}\right] \delta^2 = NT\lambda_1 \lambda_2 \delta,$$

where λ_1 and λ_2 are the mean firing rates of two neurons. Then we have

$$\begin{aligned}
E\left[\hat{\zeta}\right] =& E\left[E\left[\hat{\zeta}|\lambda_{t,i}^{(1)}, \lambda_{t,i}^{(2)}\right]\right] = \zeta \\
Var\left(\hat{\zeta}\right) =& Var\left(E\left[\hat{\zeta}|\lambda_{t,i}^{(1)}, \lambda_{t,i}^{(2)}\right]\right) + E\left[Var\left(\hat{\zeta}|\lambda_{t,i}^{(1)}, \lambda_{t,i}^{(2)}\right)\right] \\
=& \frac{\zeta}{NT\lambda_1 \lambda_2 \delta} + O\left(\frac{\zeta}{(NT\lambda_1 \lambda_2 \delta)^3}\right) \\
E\left[\log \hat{\zeta}\right] \approx& \log \zeta - \frac{1}{\zeta^2} Var\left(\hat{\zeta}\right) = \log \zeta + O\left(\frac{1}{NT\lambda_1 \lambda_2 \delta \zeta}\right) \\
Var\left(\log \hat{\zeta}\right) \approx& \frac{1}{\zeta^2} Var(\hat{\zeta}) - \frac{1}{4\zeta^2} Var\left(\hat{\zeta}\right)^2 = \frac{1}{\zeta} \frac{1}{NT\lambda_1 \lambda_2 \delta} + O\left(\frac{1}{(NT\lambda_1 \lambda_2 \delta)^2}\right).
\end{aligned}$$

We next assume that the distribution of $\log \hat{\zeta}$ is (approximately) normal, i.e., $\log \hat{\zeta} \in \mathcal{N}\left(\log \zeta, \frac{1}{\zeta} \frac{1}{NT\lambda_1 \lambda_2 \delta}\right)$, so that to get the power to equal 0.8 with type I error $.05$ we need

$$\begin{aligned}
\Phi\left(\frac{x - \log \zeta}{\sqrt{\frac{1}{\zeta} \frac{1}{NT\lambda_1 \lambda_2 \delta}}}\right) =& 0.2 \\
\Phi\left(\frac{x - \log 1}{\sqrt{\frac{1}{NT\lambda_1 \lambda_2 \delta}}}\right) =& 0.95,
\end{aligned}$$

where x is the threshold of rejecting null hypothesis $\log \zeta = 0$. We can then solve for N as the number of needed trials for detecting excess synchony:

$$N = \left\lceil \frac{1}{T\lambda_1\lambda_2\delta} \left(\frac{\Phi^{-1}(0.95) - \Phi^{-1}(0.2)/\sqrt{\zeta}}{\log \zeta} \right)^2 \right\rceil .$$